



HAL
open science

A biophysical model explains the oscillatory behaviour of immature starburst amacrine cells

Dora Karvouniari, Lionel Gil, Olivier Marre, Serge Picaud, Bruno Cessac

► **To cite this version:**

Dora Karvouniari, Lionel Gil, Olivier Marre, Serge Picaud, Bruno Cessac. A biophysical model explains the oscillatory behaviour of immature starburst amacrine cells. 2017. hal-01484133v1

HAL Id: hal-01484133

<https://inria.hal.science/hal-01484133v1>

Preprint submitted on 6 Mar 2017 (v1), last revised 28 Nov 2017 (v2)

HAL is a multi-disciplinary open access archive for the deposit and dissemination of scientific research documents, whether they are published or not. The documents may come from teaching and research institutions in France or abroad, or from public or private research centers.

L'archive ouverte pluridisciplinaire **HAL**, est destinée au dépôt et à la diffusion de documents scientifiques de niveau recherche, publiés ou non, émanant des établissements d'enseignement et de recherche français ou étrangers, des laboratoires publics ou privés.

A biophysical model explains the oscillatory behaviour of immature starburst amacrine cells

D. Karvouniari ^{*}, L. Gil [†], O. Marre [‡], S. Picaud [§]
B.Cessac [¶]

March 6, 2017

Abstract

During early development, waves of activity propagate across the retinal surface, and play a key role in the proper wiring of the early visual system. How these waves are generated by the retinal network though is still unclear. During stage II retinal waves, Starburst Amacrine Cells (SACs) exhibit an intrinsic rhythmic bursting behaviour, triggering waves of activity across the retinal surface. While several models have tried to reproduce retinal waves, none of them reproduces the rhythmic bursting of individual SACs. Here, we propose a biophysical model which reproduces certain intrinsic properties of immature bursting starburst amacrine cells. We perform a bifurcations analysis to identify the key mechanisms explaining the bursting behaviour of SACs and isolate two essential biophysical parameters controlling it; the potassium conductance g_K and the rest membrane potential V_L . This model also explains how different species can exhibit variable interburst intervals, as observed experimentally. Finally, our model provides a testable experimental prediction about the expression of voltage-dependent potassium channels along development and their role on the excitability properties of immature starburst amacrine cells.

^{*}Biovision team, Sophia Antipolis, France, email: theodora.karvouniari@inria.fr,

[†]Institut Non Linéaire de Nice, France, email: lionel.gil@inln.cnrs.fr

[‡]Institut de la Vision, Paris, France, email: olivier.marre@gmail.com

[§]Institut de la Vision, Paris, France, email: serge.picaud@inserm.fr

[¶]Biovision team, Sophia Antipolis, France, email: bruno.cessac@inria.fr.

Introduction

Retinal waves, observed in various species -turtles [17], mice [15], ferrets [7], chicks [6]- are spontaneous bursts of activity propagating in the developing retina, playing a central role in shaping the visual system and retinal circuitry. These waves emerge due to the conjunction of intrinsic cells properties (excitability and long refractoriness) and network coupling. In the retina, network interactions during development are mediated by transient networks of specific cells evolving during three consecutive stages, mainly characterized by different types of synaptic transmissions; gap junctions (stage I), acetylcholine (stage II) and glutamate (stage III) [18]. During stage II, Starburst Amacrine Cells (SACs) exhibit a spontaneous bursting behaviour, disappearing upon maturation, which triggers waves of propagating activity. Immature SACs, as clearly stated in [20], burst due to intrinsic cellular mechanisms - mainly involving voltage-gated Ca^{2+} and Ca^{+2} -gated K^+ channels- and the activity is not synaptically driven.

Features of bursting activity are observed to be quite variable across species. For example, strong differences are reported in the interburst intervals in SACs between mice ($\sim 60s$ [8]) and rabbits ($\sim 20s$ [20]), suggesting potentially different mechanisms for wave triggering across species [8]. However, stage II waves are initiated by the same cell type, SACs, in all species [21]. Therefore, if there is a different mechanism of stage II waves generation across species it must correspond to different physiological conditions of SACs, leading to different excitability properties. This indicates that there is a need for a theoretical modelling of SACs activity, attempting to capture a possible change in excitability upon varying some physiological parameters. In the context of mathematics, this corresponds to seek bifurcations in a realistic model of SACs.

Until now, no model has been proposed to describe the spontaneous activity of individual SACs in the immature retina, although there exist models dedicated to describe stage II retinal waves, the most recent being [16], [3] [9]. Although these models are intended to describe waves dynamics in a network of SACs, they do not exhibit bursting activity for isolated cells. Additionally, (i) their equations are not strictly bound to experimental findings and several parameter values are not biophysically justified; (ii) they require an exogeneous excitation (typically a shot noise current) in order to induce artificial depolarisations leading to wave propagation. Without this exogeneous excitation, neurons stay at rest and it is not possible to reproduce the spontaneous depolarization and bursting observed in [20]. Moreover,

the noise level needs to be fine tuned so as to reproduce experimental curves for waves size distribution [16].

In this paper, we propose a model of spontaneously bursting SACs, carefully calibrated with respect to the biophysics of SACs in immature retina, and able to reproduce the *spontaneous* intrinsic cell-autonomous rhythmic bursting observed experimentally in [20]. Moreover, we provide a mechanism for the spontaneous emergence of bursting of SACs during development using bifurcations theory. Our analysis exhibits two key biophysical parameters, the potassium conductance and the rest potential, controlling bursting. This leads us to two interesting conjectures: (i) on the wide range of interburst periods observed across species, which is explained by a simple argument in bifurcations theory, and, (ii) on the role of the potassium conductance variability, presumably related to specific potassium channels called *Kv3*, on the transient intrinsic properties of SACs excitability during development. We propose new experiments to test these theoretical findings.

The paper is organized as follows. The model and its validations are presented in the section "Results". Model predictions are presented in the section "Discussion". The main mathematical results are collected in the section "Methods". For the sake of clarity, the technical material, model equations derivation, mathematical analysis and parameters values are presented in the supporting information section.

Results

A biophysical model for bursting immature SACs

Following [20], the two key biophysical mechanisms associated to the emergence of spontaneous bursting of SACs during early development are:

- fast repetitive bursts of spikes, mainly controlled by voltage-gated Ca^{+2} channels;
- prolonged AHPs modulating fast oscillations, emitted by Ca^{+2} -gated K^{+} channels.

We model the underlying currents associated to the aforementioned SACs activity during development, with Morris-Lecar like dynamics [4] and additional currents which are detailed below. These currents are included - guided by experimental observations in [20] - so as to

generate spontaneous bursting. We mimic these currents with 5 variables whose evolution is controlled by a set of non-linear differential equations (see Methods): $V(t)$, the local membrane potential, $N(t)$, the gating variable for fast voltage-gated K^+ channels, $R(t)$ and $S(t)$, the gating variables for slow Ca^{2+} -gated K^+ channels, $C(t)$, the intracellular Ca^{2+} concentration. All parameters values and the auxiliary functions involved are found in the supporting information section S4.

Modeling bursting activity requires both excitatory and inhibitory variables, since the sustained oscillations are a result of their competition. Following experiments in [20] on specifying the ionic channels involved in the spontaneous bursting of immature SACs, we consider voltage-gated Ca^{+2} channels for the excitatory component of the intrinsic dynamics of bursting. It is important to note that [20] have shown that voltage-gated Na^+ channels do not participate in the bursting mechanism of immature SACs (bursting activity of SACs was not altered upon tetrodotoxin -TTX- application), thus, dynamics of Na^+ channels will not be considered in our model. The ionic channels related to the inhibitory component of SACs bursting have not yet been identified experimentally. However, in this work, we propose a modeling description by *fast* voltage-gated K^+ channels, based on Morris-Lecar dynamics [4], with a fast refractory variable N (see Methods, equation (5)). We have to mention that existing models which do not exhibit spontaneous bursting activity, either consider slow K^+ channels ($\sim seconds$) (Lansdell et al. [3]) or no K^+ channels at all (Hennig et al. [16]).

A slow After HyperPolarization (sAHP) K^+ current is responsible for the long refractoriness inbetween consecutive bursts. The modelling of this current is based on the observation in [20] that sAHP in SACs resembles SK channel currents, similar to the slow AHP currents reported in hippocampal pyramidal neurons in [2]. The modeling structure of such currents is originally inspired by Hennig et al. model [16], with strong variations in the equations, based on biophysical and experimental arguments (See the supporting information section S1 for the detailed equations derivation). It is found in [20] that the sAHP current, I_{sAHP} , is mediated by Ca^{+2} -gated K^+ channels. Our modeling is based on [11], where they analyse the mechanism of the opening Ca^{+2} -gated K^+ channels. Two steps are involved: a) Four ions of Ca^{+2} , bind to the protein Calmodulin, forming the complex CaM (saturated Calmodulin) ; b) CaM binds to each of the four CaM-binding domains on the intracellular subunit of the channel to open it. The variable R models the fraction of bounded terminals, thus, we need four terminals to open the channel. In other words, the corresponding conductance is $g_{sAHP}R^4$, where g_{sAHP} is the maximum

sAHP conductance. The full dynamics of the variable R is given in Methods.

Putting together all the above mechanisms described in our model, we propose a biophysical mechanism which explains the sustained bursting in immature SACs (see bifurcations analysis below). SACs are in a regime where they can oscillate spontaneously. As the burst starts the intracellular calcium load C increases through the increase of the voltage V . Therefore, the effect of the sAHP controlled by the variables R , S and C , increases up to a point that oscillations stop, reaching a steady state where the level of the voltage is quite lower. As a consequence, intracellular calcium concentration C unloads, I_{sAHP} decreases, until we reach a state where the effect of sAHP is small and oscillations start again. In Fig 1, we show the behaviour of the key state variables of our model illustrating the proposed biophysical mechanism for the spontaneous sustained oscillations in immature SACs.

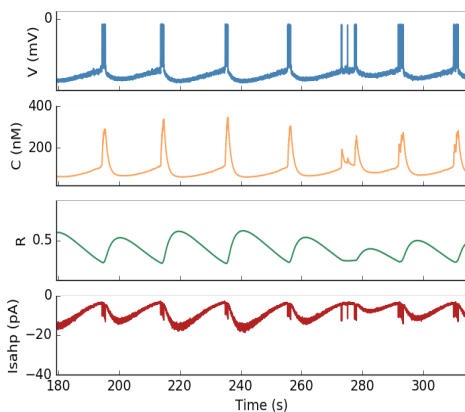


Figure 1: **Simulated dynamics of individual SACs** *Blue*. Voltage ($V(t)$) bursting for isolated SAC in the presence of additive noise. *Orange*. Intracellular Calcium ($C(t)$) Loading/Offloading Mechanism. *Green*. sAHP conductance ($g_{sAHP}(t)$). *Red*. sAHP current ($I_{sAHP}(t)$).

Characterizing the effect of noise on the interburst intervals. In [20], recordings show that the bursting periods of SACs are not regular. In contrast, the deterministic dynamics of our model leads to completely regular bursting activity (results not shown). However, this regularity breaks in the presence of a Brownian noise, added to the dynamics of the voltage V (see Fig 1 and Eq 1). We observe that

the bursting period distribution changes, while varying the noise standard deviation σ . For low noise, dynamics has fluctuations around the deterministic trajectory with little effect during the bursting phase. In contrast, low additive noise during the slow (after-hyperpolarization) dynamics, is enough to anticipate (or delay) the start of a burst. Overall, the presence of noise, regardless of its amplitude, has a drastic impact on the shape of the interbursts intervals distribution, which is represented in Fig 2. Numerically we define an interburst burst interval by a simple thresholding method, which is controlled by a Ca^{+2} concentration threshold.

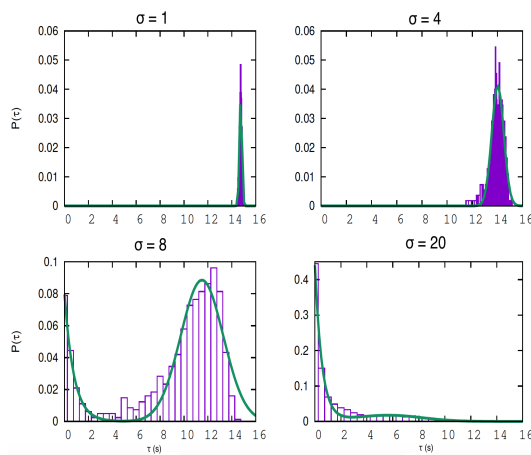


Figure 2: **Histogram of bursting periods for different noise levels.** *Top Left.* $\sigma = 1 \text{ pA ms}^{-1/2}$. *Top Right.* $\sigma = 4 \text{ pA ms}^{-1/2}$. *Bottom Left.* $\sigma = 8 \text{ pA ms}^{-1/2}$. *Bottom Right.* $\sigma = 20 \text{ pA ms}^{-1/2}$. Green curves corresponds to fit either by a Gaussian (Top Left, top right), a decaying exponential (bottom right), or a linear combination of the two (Bottom left) corresponding to a crossover between two regimes.

On the experimental side, due to the lack of sufficiently large samples, interburst intervals distributions are not well defined; thus it makes the comparison with theoretical results hard to interpret. Particularly, in [20] (Fig 3a, b), the authors compute the histogram of the bursting period for immature rabbits SAC for ~ 65 cells. Thus, the exact shape of the distribution is not sharply defined experimentally. However, a conclusion that could be drawn from the histogram measured in [20], is that it could certainly not be approximated by an exponential distribution, observed in our case for $\sigma > 8 \text{ pA ms}^{-1/2}$, regardless the small size of statistical sampling. This argument, provides us with an upper bound on the level of noise, defined in our simulations by σ , which should be no greater than $8 \text{ pA ms}^{-1/2}$.

The role of the potassium conductance in bursting activity

In [20], the authors propose that the ionic channels mainly involved in the bursting activity of SACs during early development, are voltage-gated Ca^{+2} channels. In their corresponding experiment [20], it is shown that by applying a short current pulse (150 pA for 60 ms) to individual immature SACs it is possible to control artificially the triggering of fast oscillations upon the duration of the stimulation. Also, upon the pharmacological application of Cd^{+2} , which blocks all Ca^{+2} related channels (voltage-gated Ca^{+2} and sAHP), they show that no oscillatory activity is triggered upon stimulation, but only a raise in the plateau of the level of the voltage. However, in [20], the type of ionic channels contributing to the inhibitory component of the bursting activity is not identified.

With our model, we are able to reproduce reliably the result of the described experiment, by also taking into account the dynamics of fast K^+ channels. Particularly, we are able to simulate the emergence of fast oscillations during a short current pulse, with an AHP phase after the end of the pulse (see green curve in Fig 3). We emulate as well, the disappearance of the oscillations observed by [20], upon blocking all Ca^{+2} related channels (voltage-gated Ca^{+2} and sAHP), setting the corresponding conductances to zero (see orange curve in Fig 3).

To further investigate the role of voltage-gated K^+ channels in the mechanism of bursting activity, we show with simulation that no oscillations are exhibited without the presence of fast K^+ channels, but only a rise from the rest state in the voltage plateau during the current pulse. This suggests that voltage-gated Ca^{+2} channels alone are not sufficient to produce spontaneous bursting activity. Overall, we propose that the inhibitory component of the subthreshold fast oscillations observed in immature SACs could be driven fast voltage-gated K^+ channels.

SACs in vertebrate retina are shown to lose their ability to spontaneously burst, once they reach a certain stage of development, which varies upon species. In order to investigate the mechanisms undergoing this change in excitability of SACs upon maturation, Zheng et al. 2006 [20], performed experiments on E29-P28 rabbit retinas, where they found that the spontaneous intrinsic bursting remained in SACs until P4 and became undetectable after P6. Under the assumption that neural properties changing upon maturation can be potentially partially restored under pharmacological manipulation, they treat P8 and P22 retinas with chemical agents to reinduce bursting activity.

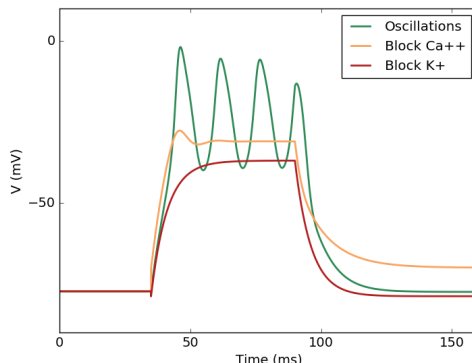


Figure 3: *Green.* Reproducing fast subthreshold oscillations and subsequent AHP emulating the experiment of [20]. Application of a current step pulse of 150 pA for 60ms . *Orange:* Oscillations disappear when Ca^{+2} related conductances are set to zero. *Red.* Blocking the oscillations upon setting the voltage-gated K^{+} conductance to zero.

They show that in order to reinitiate bursting activity in further developed SACs, it is crucial to both i) block all synaptic connections, especially inhibition and ii) decrease the conductance of the fast K^{+} channels g_K (TEA sensitive) upon pharmacological manipulation. It is worth noting that, at P8, complete pharmacological isolation of SACs is not enough to restore bursting, indicating that at this point of development, bursting is not suppressed by inhibitory synaptic input. This suggests that upon maturation bursting is suppressed by alterations in the intrinsic properties of individual SACs. In the same preparation (P8 isolated SACs), the induction of TEA resulted in restoring bursting activity in isolated mature SACs.

In order to capture this pharmacologically dependent change in excitability of SACs with our model, we vary the conductance of the fast K^{+} channels g_K (cells are isolated in the model). We observe that oscillations stop (Fig 4 top green trace) for a moderate increase of g_K (8 nS to 20 nS). Decreasing afresh the value of the K^{+} conductance g_K , evidently restores bursting (Fig 4 green bottom trace). Therefore, our model suggests that with a single key parameter, the fast potassium conductance g_K , we can control the loss of excitability of SACs upon maturation.

Upon further maturation, the restoration of bursting in P22 SACs (late stage III-before eye-opening) depends on the interplay between the change of the intrinsic properties of K^{+} channels strong inhibition (TEA application) and blocking the strong inhibitory input induced by other amacrine cells at this phase [20]. Neither of these conditions

suffices alone for the bursting restoration. Our model, emulates the effect of the inhibitory synaptic input with a constant negative external current I_{ext} . Bursting re-initiation is successful with our equations, by setting the current I_{ext} to zero and at the same time decreasing the conductance of the K^+ channels g_K .

To illustrate the reliable reproduction of the experimental findings on the transient excitability of SACs along development in [20] (Fig 7), we simulate the pharmacological manipulation they performed at all three separate ages; $P4$, $P8$ and $P22$ in Fig 4.

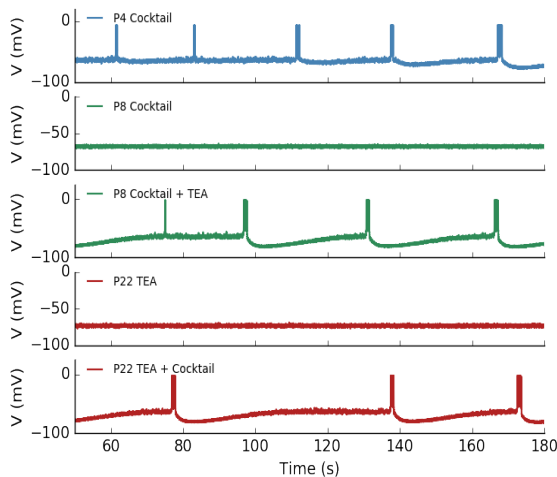


Figure 4: *Blue.* Modeling the bursting activity of isolated P4 SAC, $g_K = 8nS$. *Green top.* Modeling P8 isolated SAC where we see no bursting activity, $g_K = 20nS$. *Green bottom.* Decreasing $g_K = 9nS$ we restore oscillations. *Red top.* Modeling P22 coupled SAC where there is no bursting activity upon treatment with TEA. A constant external current $I_{ext} = -10pA$ is applied to coarsely mimic the gabaergic inhibitory input to SAC at this stage of development. *Red bottom.* Restoration of bursting at P22 by removing all inhibitory synaptic connections, $I_{ext} = 0pA$. Removing inhibition from mature amacrine circuitry, along with blocking a subfamily of K^+ channels with TEA, is enough to reinitiate bursting activity, $g_K = 10nS$.

Explaining the wide range of interburst intervals across species by a unique mechanism

Spontaneous bursting activity in immature SACs has been consistently observed across various species i.e. mice, rabbits, chicks, turtles etc., although, the measured bursting periods strongly vary [17], [15],

[7], [6]. This experimental observation rises the question on whether there exists a single underlying mechanism which could explain such variability across species, instead of possibly several corresponding mechanisms for each different species.

In order to address this question, we compute how the mean inter-burst interval (IBI) τ , changes upon the variation of the rest membrane potential V_L . The rest state is an explicit function of parameters, mainly dominated by the V_L . The variation of V_L allows us to characterize the mean bursting period of SACs, under normal physiological conditions of the rest membrane potential ($\sim -70mV$) and also within an extended interval of V_L . As a result, we show that the mean inter-burst interval of SACs $\langle \tau \rangle$ increases monotonously as V_L decreases, following an hyperbola -see Fig 5, yellow trace- whose form has been derived analytically (see Appendix and Fig 5, blue trace). We also observe a sharp transition from a bursting to a non-bursting regime, where $\langle \tau \rangle = 0$, which corresponds to the loss of SACs excitability.

Based on the shape of our theoretical curve, we show that the mean inter-burst interval exhibits a *strong asymptotic behaviour* around a very narrow regime of the rest potential ($V_L = -71$ mV, $\delta V_L \sim 2$ mV). This means that depending on slight variations of physiological conditions ($\delta V_L \sim 2$ mV) a SAC could exhibit very variable bursting periods, explaining how different species exhibit variability in the IBI of immature SACs. In order to further illustrate this, we show the mean IBI for different species found in the literature, crossing our curve within the narrow asymptotic region. For turtles and chicks the actual values of interbursts intervals (IBI) were not found in the literature, but only their interwave intervals (IWI) instead. In order to extrapolate the IBI for these species, we used a common constant scaling factor of 3, based on the ratio between IBI and IWI for rabbits and mice found in [20] and [8] respectively.

Besides this narrow regime where we observe the asymptotic behaviour, we show that a decrease of V_L results to a sharp disappearance of bursting activity, which means that bursting activity stops after a well defined threshold of V_L . Decreasing V_L is equivalent to add a constant negative current in the model, which could be mimicking a change in the intrinsic inhibitory ionic currents of individual SAC or external inhibitory inputs from other layers of the retina upon maturation. These two factors should drive the disappearance of bursting activity and subsequently the loss of SACs excitability.

On the other hand, an increase of V_L leads to a gradual decrease of the mean IBI towards zero, meaning that in this regime of parameters, SACs tend to burst repeatedly, without a refractory period. This sce-

nario is not observed under normal physiological conditions, but could be tested experimentally by varying V_L pharmacologically. On the experimental side, in [21], it is found that the bursting period increases upon maturation (experiment in P1-P2 rabbit SAC), which could be linked to a change of intrinsic properties of SACs during development. However, it is not clear how synaptic inhibition acts on the disappearance of bursting activity of immature SAC across species. Taken together, the hyperbolic behaviour of the mean IBI within a narrow range suggests that bursting activity in immature SACs share a common mechanism across species.

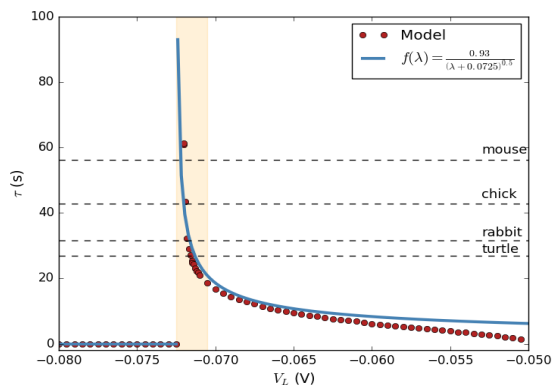


Figure 5: *Orange*. Computing the dependence of $\langle \tau \rangle$ upon the variation of V_L with our model. *Blue*. Fit of the simulated data with the curve $\frac{K}{2\sqrt{I_{ext}-I_c}}$ for $V_L > -72mV$, where I_c is a critical value depending on noise and K a constant (see Supporting Information Section S4). *Red*. Values of experimentally measured interburst intervals for different species mapped to our results (see text).

Discussion

In this paper we have proposed a biophysical model for spontaneous bursting of SACs, one of the key ingredients for the initiation of stage II retinal waves. Although this model has many parameters, bifurcations analysis allows us to exhibit two key parameters, g_K or V_L , controlling important aspects of dynamics, in direct links with experiments. This leads us to propose several conjectures and possible experiments, directly inspired from the model analysis. We would like now to develop other aspects, not considered in the main text.

A conjecture on the role of the potassium conductance and Kv_3 channels in the loss of SACs excitability upon maturation.

As we have shown with our model, the conductance g_K of the fast K^+ channels is the key parameter to suppress the bursting activity of SACs. However, the exact type of potassium channels involved has not been identified yet. In [20], the authors show that in order to reinitiate bursting activity in further developed SACs, it is crucial to decrease the conductance of the K^+ channels which are TEA-sensitive. In mature SACs, [14] and [1] have identified TEA-sensitive potassium channels which belong to the Kv_3 family. On top of describing the cellular mechanisms found by [20], we suggest a unique role of Kv_3 channels in the transient properties of SAC excitability during development. The expression of fast K^+ Kv_3 channels during development and their possible role in immature SACs excitability has not yet been investigated experimentally, to our best knowledge.

In more detail, we propose that, during early development ($< P6$), Kv_3 channels are under-expressed, allowing a competition between inhibition (K^+) and excitation (Ca^{+2}), leading SACs to burst (see Fig 4, blue trace). Upon maturation, the expression of these channels could evolve increasingly, leading to stronger inhibition, dominating fully the competition of inhibitory/excitatory channels, by suppressing oscillations completely. In our equations, an increase of Kv_3 channels conductance g_K leads to blocking the oscillations completely (see Fig 4, green top trace), suggesting, that the development of fast Kv_3 channels could be the transient process that leads to a complete loss of excitability of mature SAC.

Note that only one of the two subtypes of voltage gated K^+ channels of the Kv_3 family found in mature SAC [14] are TEA sensitive. Indeed, two types of currents are found in mature SACs: i) I_K , delayed rectifier currents, sensitive to TEA and ii) I_A A-type currents, sensitive to 4-amino- pyridine (4AP), emitted by subunits $kV3.3$ and $kV3.4$ [14]. On these bases, we propose that the specific type of potassium channels responsible for the spontaneous bursting activity during development and eventually its loss upon maturation, is the $Kv3.3, 4$ subtype.

Our study results in proposing a quantified method, experimentally testable, to restore bursting activity in fully developed SACs. It could be interesting to test experimentally the evolution of the expression of these channels during development. Our results indicate that the level of their expression would increase gradually upon maturation, which essentially means that the conductance of these channels

would increase as well. This type of experiment would elucidate the exact role of $Kv3$ channels in the intrinsic properties of the excitability of SACs.

Coupled bursting SACs produce retinal waves

In this work, our modeling concerns individual neuron dynamics, describing in detail the cellular mechanisms leading to bursting. This activity is crucial for the emergence of propagating wave activity. A next step of our work will consist of studying a network of coupled SACs to elucidate the mechanisms for propagating spatio-temporal patterns in the developing retina at stage II, capturing the third ingredient necessary for the emergence of retinal wave. This could provide a strict mathematical framework to study retinal waves initiation, propagation and eventual disappearance, as well as a quantitative characterization of waves in order to classify and further characterize them. However, in contrast to existing models, the introduction of bursting significantly complexifies the dynamics and the mathematical analysis, especially if one considers in details the synaptic coupling via acetylcholine, which is not a mere diffusion process, as assumed in [3]. This is the object of a forthcoming paper.

Methods

The Model

Our model has 5 variables whose evolution is controlled by non linear differential equations: $V(t)$, the local membrane potential, $N(t)$, the gating variable for fast K^+ channels, $R(t)$ and $S(t)$, the gating variables for slow Ca^{2+} -gated K^+ channels, $C(t)$, the intracellular Ca^{2+} concentration. All parameters values and the auxiliary functions involved are found in the supporting information section S3. Equations (1), (5), (8), (9), (7) below constitute the dynamical system that we now analyse. The equation for the voltage V is:

$$C_m \frac{dV}{dt} = I_L + I_C + I_K + I_{sAHP} + \sigma \xi_t, \quad (1)$$

where C_m is the membrane capacity and ξ_t is a white noise whose amplitude is controlled by σ . This weak additive noise (mean std $\sim 4pA$) is used to mimic the natural background noise of biological systems.

The term:

$$I_L = -g_L(V - V_L), \quad (2)$$

is the leak current.

The terms I_C and I_K , respectively corresponding to Calcium and Potassium currents, are generating the fast Ca^{+2} oscillations. These currents are controlled by a Morris-Lecar model [4]. The voltage-gated Ca^{+2} current is:

$$I_C = -g_C M_\infty(V)(V - V_C). \quad (3)$$

$g_C M_\infty(V)$ is the voltage dependent conductance of the Ca^{+2} channel (see supporting information section S3).

$$I_K = -g_K N(V - V_K). \quad (4)$$

$$\tau_N \frac{dN}{dt} = \Lambda(V)(N_\infty(V) - N), \quad (5)$$

where $\Lambda(V)$ and $N_\infty(V)$ are given by Eq (22), (23) in supporting information section S4.

The expression for the sAHP current is given by:

$$I_{sAHP} = -g_{sAHP} R^4 (V - V_K). \quad (6)$$

We have finally 3 differential equations to generate the sAHP conductance:

$$\tau_C \frac{dC}{dt} = -\frac{\alpha_C}{H_X} C + C_0 - \delta_C g_C M_\infty(V)(V - V_C), \quad (7)$$

equation for internal Calcium concentration;

$$\tau_S \frac{dS}{dt} = \alpha_S C^4 (1 - S) - S, \quad (8)$$

equation for saturated Calmodulin concentration;

$$\tau_R \frac{dR}{dt} = \alpha_R S (1 - R) - R, \quad (9)$$

equation for the fraction of open Ca^{+2} -gated K^+ channels. These equations are justified in supporting information section S1.

Bifurcation analysis

Bursting is an alternance between a rest state and repetitive firing, often modulated by slow voltage- or Ca^{+2} - dependent processes [13]. In our case, the joint fast dynamics of Ca^{+2} and K^+ channels generates fast oscillations while the slow AHP, mediated by Ca^{+2} gated

K^+ channels, modulates slow oscillations, [20]. The conjunction of these two mechanisms generate bursting as we now explain.

For this, we perform a slow-fast time scale analysis. The variable V, N evolve with a fast time scale under the influence of the slow current I_{sAHP} driven by slow variables C, S, R (see supporting information section S2). Due to the time scales separation, it is relevant to make a bifurcation analysis of the fast V, N dynamics, in the presence of a constant external current I_{ext} used as a bifurcation parameter. The bifurcations diagram is represented in Fig 6 (drawn using PyCont [5]), where we have explored a wide range of variation of I_{ext} , (-100 to $+300$ pA). Red lines correspond to stable fixed points, dashed-dot line are neutral saddle points and dashed line represents unstable fixed points. We also show a zoom of this diagram in Fig 7, as the range of I_{ext} where bursting takes place is narrow.

When $I_{ext} < I_{H_c} \sim -5.83$ pA, there is stable rest state (lower, red branch in Fig 6, 7), where $V_{rest} \in [-70, -60]$ mV, coexisting with two unstable fixed points (middle and upper branch). For $I_{ext} = I_{H_c}$ there is an homoclinic bifurcation giving rise to a stable limit cycle. In the range $I_{ext} \in [I_{H_c}, I_{SN_1}]$, where $I_{SN_1} \sim -3.7$ pA, the stable rest state (lower branch) coexists then with a stable limit cycle, corresponding to fast oscillations, and an unstable fixed point (middle branch). When $I_{ext} = I_{SN_1}$ the stable rest state coalesces with the middle unstable branch and both disappear with a saddle-node bifurcation (SN_1). For $I_{ext} > I_{SN_1}$ the dynamics has only attractor, the limit cycle, corresponding to fast oscillations. This cycle eventually disappears by a Hopf bifurcation at $I_{ext} = 250$ pA. This value of external current is quite beyond the range of plausible values during the bursting activity of SACs though.

From a dynamical systems perspective, there are two important bifurcations associated with bursting: a) bifurcation of the rest state that leads repetitive firing and b) bifurcation of a spiking attractor that leads to a rest state [13]. There are two possible types of bifurcations linked to such type of behaviour (i) Homoclinic saddle-node bifurcation and (ii) Hopf bifurcation and. We have therefore shown that (i) holds in our case. The first bifurcation associated to the breaking of the rest state is the saddle-node bifurcation. The "spiking attractor", here the limit cycle, is created by an homoclinisation. According to the classification of bursting made by Izhikevich in [13], this corresponds to a "square-wave" point-cycle planar burster.

To summarize we have shown that SACs have the capacity to switch between two distinct states corresponding to a *stable fixed point* and a *limit cycle* respectively and exhibit *self-sustained spontaneous* bursting behaviour. SACs spontaneously produce fast oscillations when

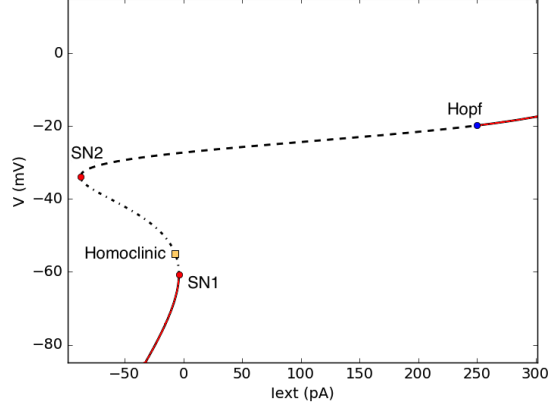


Figure 6: Bifurcation diagram of the fast dynamics (Eq (20) in supporting information section S2) when the constant current I_{ext} is varied in a wide range. *Red*. Stable fixed points. *Dashed-dot line*. Neutral saddle points. *Dashed line*. Unstable fixed points. SN stands for Saddle-Node bifurcation. For further references on this terminology see [12].

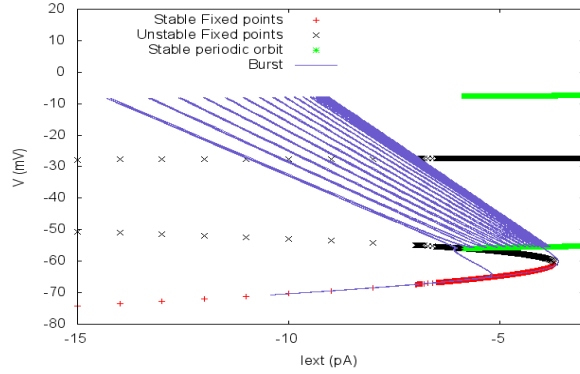


Figure 7: Representation of bursting in the plane $I_{ext} - V$ in relation with the bifurcation diagram of figure 6 (zoom). In addition, we observe the trajectory of a burst in the plane ($I_{sAHP} \equiv I_{ext}, V$) (purple). In the fast oscillations regime V is varying periodically, with a fast period, inducing a fast variation of the term $V - V_K$ in the sAHP current, explaining the diagonal motion. The conductance $g_{sAHP}R^4$ is varying slowly, with the time scale of R , explaining the slow leftwise shift of the trajectory until the homoclinic bifurcation point is reached.

$I_{sAHP} = 0$ summarized in Fig 7. Here, red and black lines correspond to stable and unstable fixed points and green line represent the amplitude of the limit cycle. The purple trace is the trajectory of a burst in the plane ($I_{ext} = I_{sAHP}, V$).

Being in a high voltage state, Ca^{2+} loads, leading to a raise of sAHP current. This corresponds, in the bifurcation diagram, to a motion toward negative current values. This motion goes on until the cell reaches the homoclinic bifurcation where oscillations stop. I_{sAHP} is high now, leading to the hyperpolarization phase. Then, because voltage is low, $[Ca^{2+}]$ decreases and I_{sAHP} drops down. Eventually, SAC crosses the SN_1 bifurcation point and starts bursting again. In this scenario, cells burst therefore periodically, with a frequency controlled by the characteristic times τ_R, τ_S of variables R and S respectively.

Acknowledgments

This work was supported by the French ministry of Research and University of Nice (EDSTIC). We warmly acknowledge Matthias Hennig and Evelyne Sernagor for their invaluable help.

References

- [1] Ozaita A., Petit-Jacques J., Volgy B., Ho C. S., Joho H., S. A. Bloomfield, and B. Rudy. A unique role for kv3 voltage-gated potassium channels in starburst amacrine cell signaling in mouse retina. The Journal of Neuroscience, 33(24):7335–7343, 2004.
- [2] H. J. Abel, J.C.F. Lee, J. C. Callaway, , and R. C. Foehring. Relationships between intracellularneocortical pyramidal neurons calcium and afterhyperpolarizations in neocortical pyramidal neurons. J Neurophysiol, 2004.
- [3] Lansdell B, Ford K, and Kutz JN. A reaction-diffusion model of cholinergic retinal waves. PLoS Computational Biology, 10(12):1–14, 2014.
- [4] Morris C and Lecar H. Voltage oscillations in the barnacle giant muscle fiber. BIOPHYS. J., 35:193–213, 1981.
- [5] Robert Clewley. Hybrid models and biological model reduction with pydstool. PLoS Computational Biology, 2012.
- [6] Sernagor E., Eglén S.J., and O’Donovan M.J. Differential effects of acetylcholine and glutamate blockade on the spatiotemporal dynamics of retinal waves. The Journal of Neuroscience: The Official Journal of the Society for Neuroscience., 20:RC56, 2000.
- [7] Marla B. Feller, Daniel A. Butts, Holly L. Aaron, Daniel S. Rokhsar, and Carla J. Shatz. Dynamic processes shape spa-

- tiotemporal properties of retinal waves. Neuron, 19(2):293 – 306, 1997.
- [8] Kevin J. Ford and Marla B. Feller. Assembly and disassembly of a retinal cholinergic network. Visual Neuroscience, 29:61–71, 1 2012.
- [9] Keith B Godfrey and Nicholas V Swindale. Retinal wave behavior through activity-dependent refractory periods. PLoS Comput Biol, 3(11):e245, 11 2007.
- [10] Michael Graupner. A theory of Plasma Membrane Calcium pump function and its consequences for presynaptic calcium dynamics. PhD thesis, Master’s thesis, TU Dresden, Dresden, 2003.
- [11] Michael Graupner, Frido Erler, and Michael Meyer-Hermann. A theory of plasma membrane calcium pump stimulation and activity. Journal of biological physics, 31(2):183–206, 2005.
- [12] J. Guckenheimer and Ph. Holmes. Non linear oscillations, dynamical systems, and bifurcation of vector fields. Springer-Verlag, 1983.
- [13] E.M. Izhikevich. Dynamical Systems in Neuroscience: The Geometry of Excitability and Bursting. The MIT Press, Cambridge, MA, 2007.
- [14] Kaneda M, Ito K, Morishima Y, Shigematsu Y, and Shimoda Y. Characterization of voltage-gated ionic channels in cholinergic amacrine cells in the mouse retina. J Neurophysiol, 2007.
- [15] A. Maccione, M. Hennig M., M. Gandolfo, O. Muthmann, J. van Coppenhagen, S. Eglén, L. Berdondini, and E. Sernagor. Following the ontogeny of retinal waves: pan-retinal recordings of population dynamics in the neonatal mouse. J Physiol, 485:1545–1563, 2014.
- [16] Hennig MH, Adams C, Willshaw D, and Sernagor E. Early-stage waves in the retinal network emerge close to a critical state transition between local and global functional connectivity. J Neurosci, 2009.
- [17] E. Sernagor and N. Grzywacz. Spontaneous activity in developing turtle retinal ganglion cells: Pharmacological studies. J Neuroscience, 19, 1999.
- [18] Evelyne Sernagor and Matthias Hennig. Retinal Waves: Underlying Cellular Mechanisms and Theoretical Considerations. Elsevier, 2012.

- [19] Ji-jian Zheng, Seunghoon Lee, and Z.Jimmy Zhou. A developmental switch in the excitability and function of the starburst network in the mammalian retina. Neuron, 44(5):851–864, 2004.
- [20] Jijian Zheng, Seunghoon Lee, and Z. Jimmy Zhou. A transient network of intrinsically bursting starburst cells underlies the generation of retinal waves. Nat Neurosci, 9(3):363–371, 2006.
- [21] Z. Jimmy Zhou. Direct Participation of Starburst Amacrine Cells in Spontaneous Rhythmic Activities in the Developing Mammalian Retina. J. Neurosci., 18(11):4155–4165, June 1998.

Supporting Information

S1: Deriving sAHP dynamics

To our best knowledge, the ionic channels type involved in sAHP for immature stage II SAC is not precisely known. However, Zheng et al. argue in [20] that these channels could share characteristics with SK channels, thoroughly studied for pyramidal neurons by Abel et al in [2]. On this basis we modelled SK channels dynamics. SK channels have four subunits associating to form a tetramer. The SK channel gating mechanism is controlled by intracellular Calcium levels. The precise mechanism is: (i) Calcium binds to the protein calmodulin forming the complex CaM where 4 ions Ca 2+ are fixed to calmodulin; (ii) CaM binds to a SK channel terminal to open it; (iii) 4 terminals must be open to let the SK channel open. We now model these different steps.

Saturated Calmodulin production. The set of kinetic equations leading to CaM formation is widely described in M. Graupner's work [10, 11]. This is a cascade of equations that we summarize in one kinetic equation, from free Calmodulin, M , to the saturated one, CaM .

Let us call k_{ass} ($M^{-4}s^{-1}$) and k_{diss} (s^{-1}) respectively association and dissociation constants of Calmodulin. Set $K_d^4 = \frac{k_{diss}}{k_{ass}}$. If we call $M_0 = [M] + [CaM]$ the total Calmodulin concentration, and $S = \frac{[CaM]}{M_0}$ the fraction of saturated Calmodulin, we have $\frac{[M]}{M_0} = 1 - S$ and we obtain a kinetic equation:

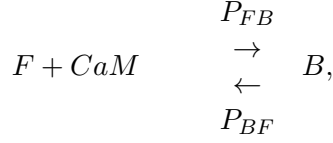
$$\frac{dS}{dt} = k_{ass}C^4(1 - S) - k_{diss}S.$$

where C is the intracellular Calcium concentration. Setting $\tau_S = \frac{1}{k_{diss}}$ and $\alpha_S = \frac{k_{ass}}{k_{dis}} = \frac{1}{K_d^4}$ we arrive at:

$$\tau_S \frac{dS}{dt} = \alpha_S C^4 (1 - S) - S. \quad (10)$$

Note equation (8) has a similar form to the one proposed by Henig et al. in [16]. However, in their model our term C^4 is replaced by $\frac{C^4}{K_d^4 + C^4}$ which is hardly interpretable in terms of kinetics.

Binding of Calmodulin to SK terminals. This corresponds to a reaction:



where F is the density of free terminals, B the density of bounded terminals, P_{FB} (P_{BF}) the transition rate from free to bound (bound to free).

Calling R the fraction of bounded terminals, $\tau_R = \frac{1}{P_{BF}}$, $\alpha_R = \frac{P_{FB}}{P_{BF}}$ we end up with a kinetic equation:

$$\tau_R \frac{dR}{dt} = \alpha_R S(1 - R) - R = \alpha_R S - (1 + \alpha_R S)R. \quad (11)$$

Equation (9), is similar to eq. (3) in [16] ($\tau_R \frac{dR}{dt} = (\alpha C + S)(1 - R) - R$), with a remarkable difference: in our model there is no direct dependence on Calcium concentration whereas the term αC in [16] corresponds to a direct binding of Ca^2 to a terminal. Note that, taking the quite large value of the parameter α (2400) considered by these authors, their equation is essentially equivalent to $\tau_R \frac{dR}{dt} = \alpha C(1 - R) - R = \alpha C - (1 + \alpha C)R$ with a steady state $R = \frac{\alpha C}{1 + \alpha C}$ very close to 1 whenever αC is quite larger than 1. In this case, S plays essentially no role.

Finally, since R is the probability that a terminal is open and since 4 terminals must be open to let the SK channel open, the sAHP conductance is $g_{sAHP}R^4$.

Calcium concentration Both variables R and S are driven by intracellular Ca^2 concentration dynamics, given by:

$$\tau_C \frac{dC}{dt} = -\frac{\alpha_C}{H_X} C + C_0 - \delta_C g_C M_\infty(V)(V - V_C) \quad (12)$$

Equation (12) is a linear approximation of a more complex equation ((15) below). This equation is similar to Hennig et al (eq. (5)) with two notable differences: (1) We have added a rest concentration C_0 avoiding unphysical situations where C can become negative; (2) the value of parameters are different.

Calcium concentration dynamics. The Calcium current crossing a membrane section results from the opening of gates in ionic channels. Following [10] the equation for Ca concentration is (adapted with our notations):

$$\frac{dC}{dt} = \frac{G}{n_{Ca}F} \left[\frac{I_C}{S} - J_X(C) - J_p(C) + L \right] \frac{1}{1 + \frac{dCa_{bound}}{dC}}. \quad (13)$$

Here $G = \frac{S}{V} = 6 \mu m^{-1} = 6 \times 10^5 dm^{-1}$ is the surface to volume ratio that accounts for the localisation of the channels at the surface of the membrane, $n_{Ca} = 2$ is Calcium valence and $F = 96500 C mol^{-1}$ is the Faraday number. $\frac{dCa_{bound}}{dC}$ corresponds to a quasi-steady-state approximation for the Calcium buffering where the bound Calcium concentration (on Calmodulin) Ca_{bound} is adapted instantaneously to the free Calcium concentration C at each time. Since we have no way to estimate $\frac{dCa_{bound}}{dC}$ we shall consider it is a constant we shall set $\frac{1}{1 + \frac{dCa_{bound}}{dC}} \equiv K_{bound}$. To alleviate notations we set:

$$r = \frac{G K_{bound}}{n_{Ca} F}. \quad (14)$$

The first term in eq. (13), $r \frac{I_C}{S}$ corresponds to an increase of internal Ca^{2+} concentration upon Calcium influx (current $I_C(V)$) generated by spikes or, in experiments, by voltage clamp. As $V_{Ca} = 50mV$ this current is positive unless $V > V_{Ca}$.

The second term is $-r J_X(C)$, where

$$J_X(C) = \rho_X I_X \frac{C}{H_X + C},$$

is the efflux current density through Sodium-Calcium Exchanger (NCX). It corresponds to an outward through NCX exchangers, contributing to restoring the initial Ca concentration. Here, ρ_X is the surface density of the NCX membrane proteins. We take $\rho_X = 100 \mu m^{-2} = 10^{12} dm^{-2}$ (from [11]). $I_X = 4.8 \times 10^{-19} C ms^{-1} = 4.8 \times 10^{-16} C s^{-1}$ is the maximum ionic flux through a single NCX channel. This corresponds to 3 + charges ($1.5 Ca^{2+}$) per ms ; $H_X = 1.8 \mu M = 1.8 \times 10^{-6} M$ is the half activation concentration [10].

Also, in (13), $J_p(C)$ is the current density of Ca pumps. We shall neglect this term from now on. Finally, L is the leakage surface current density representing the residual conductivity of the plasma membrane. We have not been able to find its value in the literature.

To summarize eq. (13) becomes:

$$\frac{dC}{dt} = r \left[\frac{I_C}{S} - \rho_X I_X \frac{C}{H_X + C} + L \right]. \quad (15)$$

We also assume that NCX current term is approximated by a linear term. This is valid if one assumes that Calcium concentration $C \ll H_X$ which is the case in our simulations.

In order to match (15) with the form (12) ((7) in the text), we set:

$$\frac{\alpha_{Ca}}{\tau_{Ca}} = r\rho_X I_X; \quad (16)$$

$$\frac{\delta_{Ca}}{\tau_{Ca}} = \frac{r}{S}; \quad (17)$$

$$\frac{C_0}{\tau_{Ca}} = rL. \quad (18)$$

$$(19)$$

S2: Rescaled equations and Multi-time scale analysis

The dynamical system (1), (5), (8), (9), (7) has 3 characteristic times scales: fast variables V, N (of order ms); medium C (of order s); slow R, S (of order 10 s). In order to make explicit this time-scales separation we set $\tilde{g}_X = \frac{g_X}{|g_L|}$ for conductances ($X = C, K, sAHP, A$); $\tau = \frac{C_m}{g_L}$; $\tilde{t} = \frac{t}{\tau}$; $\tilde{\tau}_X = \frac{\tau_X}{\tau}$, where $X = N, C, R, S$. This gives:

$$\left\{ \begin{array}{l} \tau_L \frac{dV}{dt} = -\tilde{g}_L(V - V_L) - \tilde{g}_C M_\infty(V)(V - V_C) \\ \quad \quad \quad - \tilde{g}_K N(V - V_K) - \tilde{g}_{sAHP} R^4(V - V_K) \\ \tau_N \frac{dN}{dt} = \Lambda(V)(N_\infty(V) - N) \\ \tau_C \frac{dC}{dt} = -\frac{H_X}{\alpha_C} C + C_0 - \delta_C g_C M_\infty(V)(V - V_C) \\ \tau_S \frac{dS}{dt} = \alpha_S(1 - S)C^4 - S \\ \tau_R \frac{dR}{dt} = \alpha_R S(1 - R) - R \end{array} \right.$$

On the fast time scale, one uses the approximation $\frac{1}{\tau_X} = 0$, $X = C, S, R$, and the variables C, S, R are constant. So, fast dynamics reduces to a Morris-Lecar model (here with a fast variable N) in the presence of an additional current $I_{ext} = I_{sAHP}$ (constant):

$$\left\{ \begin{array}{l} C_m \frac{dV}{dt} = -g_L(V - V_L) - g_C M_\infty(V)(V - V_C) \\ \quad \quad \quad - g_K N(V - V_K) - I_{ext}; \\ \tau_N \frac{dN}{dt} = \Lambda(V)(N_\infty(V) - N). \end{array} \right. \quad (20)$$

S3: How the average interburst depends on the parameter I_{ext}

Here we provide an approximation for the interburst interval. We call I_{SN_1} the value of external current, in the Morris-Lecar bifurcation diagram, where the saddle node bifurcation SN_1 occurs. When $I_{ext} < I_{SN_1}$ and $\sigma = 0$, bursting stops and dynamics stays on a stable fixed point. So $I_{ext} = I_{SN_1}$ is a critical value. In the presence of noise, we can have bursting even if $I_{ext} < I_{SN_1}$, whenever noise allows the neuron to leave the stable fixed point and go in the bursting region. The probability to enter this region depends on the distance to the bifurcation point and on the noise intensity. So, the critical value of the current $I_c \equiv I_c(\sigma)$ depends on σ . In the remaining of this section we shall assume σ is small enough so that a true bursting process takes place. Indeed, when σ is too large noise dominates dynamics and the bursting loop (Ca load- sAHP increases -V decreases -Ca unload) does not take place. In the presence of noise we expect a strong variation of the period when I_{ext} approaches I_c from above. Indeed, I_{SN_1} is a saddle-node bifurcation point for the Morris-Lecar model. The normal form corresponding to this bifurcation is $\dot{x} = \mu_c - \mu - x^2$ where μ is the control parameter, μ_c is the bifurcation point, and x is the variable projecting on the central manifold [12]. In general μ is a reduced parameter that comes out for the full normal form analysis. In our case, μ this is a function of I_{ext} whereas μ_c is controlled by I_{SN_1} and the noise mean-square deviation σ . We have thus 2 fixed points $\pm\sqrt{\mu_c - \mu}$, for $\mu \leq \mu_c$. The derivative of the normal form right hand side is $-2x$. Thus, near the fixed points the flow approaches the stable fixed point (leaves the unstable fixed point) exponentially fast as $e^{\mp 2\sqrt{\mu_c - \mu}t}$, thus with a characteristic time $\frac{1}{2\sqrt{\mu_c - \mu}}$. There is thus a critical slowing down when approaching the fixed point.

When $I_{ext} < I_{SN_1}$, the interburst interval is the time to get near the stable fixed point (time t_1) and then to leave this point due to noise (time t_2). This time is proportional to $\frac{1}{2\sqrt{\mu_c - \mu}}$ and it becomes the longest time (compared to t_2) when $\mu \rightarrow \mu_c$. We expect therefore the interburst to diverge like $\frac{1}{2\sqrt{I_{ext} - I_c}}$ as $I_{ext} \rightarrow I_c(\sigma)$. When $I_{ext} \geq I_{SN_1}$, there is still an influence of I_{ext} on the interburst interval (by continuity). As we get further from I_{SN_1} though the interburst interval depends less on I_{ext} because, here, interburst is essentially controlled by the deterministic bursting loop and noise can just delay or anticipate the entrance in the bursting regime.

S4: Parameters value and auxiliary functions

Units. In all the paper, physical quantities are expressed in the units displayed in table 1.

Table 1: Dimensions of physical quantities used in the paper.

Physical quantity	Dimension
Time	ms
Potential	mV
Capacity	pF
Current	pA
Conductance	nS
Concentrations	nM

Auxiliary functions. The dimensionless auxiliary functions involved in the dynamical equations appearing in the model definition are:

$$M_{\infty}(V) = \frac{1}{2} \left[1 + \tanh\left(\frac{V - V_1}{V_2}\right) \right], \quad (21)$$

$$\Lambda(V) = \cosh\left(\frac{V - V_3}{2V_4}\right), \quad (22)$$

$$N_{\infty}(V) = \frac{1}{2} \left[1 + \tanh\left(\frac{V - V_3}{V_4}\right) \right], \quad (23)$$

Parameters. The parameters used in the model are displayed in table 2.

Calibrating parameters from experiments All parameters values are carefully calibrated with respect to biophysics, found in the literature or fitted from experimental curves in [2], [19] and [20]. Morris-lecar tuning parameters V_1 , V_2 , V_3 , V_4 were calibrated (see Fig 3), so as to reproduce the experiment of [20] (Fig 4a), where the authors investigate the ionic mechanisms of the fast oscillations. Note that the bursting regime is robust to (small) variations of these parameters (results not shown). We tuned the sAHP parameters taking into account the analogy with SK channels studied in [2] (fit not shown). Also, we note that the intensity of sAHP observed by Abel et al. in pyramidal neurons (of order 150 pA) is quite bigger than in stage

Parameter	Physical value
C_m	$22 pF$
g_L	$2 nS$
g_C	$12 nS$
g_K	$[6, 20] nS$
g_{sAHP}	$2 nS$
V_L	$[-72, -70] mV$
V_C	$50 mV$
V_K	$-90 mV$
V_1	$-20 mV$
V_2	$20 mV$
V_3	$-25 mV$
V_4	$7 mV$
τ_N	$5 ms$
τ_R	$8300 ms$
τ_S	$8300 ms$
τ_C	$2000 ms$
δ_C	$10.503 nM pA^{-1}$
α_S	$\frac{1}{200^4} nM^{-4}$
α_C	$4865 nM$
α_R	4.25
H_X	$1800 nM$
C_0	$88 nM$

Table 2: Range of values for the parameters used in the paper.

II SAC. In our model, this means a lower sAHP conductance g_{sAHP} ($g_{sAHP} = 2 nS$).